BCR affinity differentially regulates colonization of the subepithelial dome and infiltration into germinal centers within Peyer's patches

BCR affinity differentially regulates colonization of the subepithelial dome and infiltration into germinal centers within Peyer's patches

Adi Biram[1], Anneli Strömberg[2], Eitan Winter[3], Liat Stoler-Barak[1], Ran Salomon[1], Yoseph Addadi[4], Rony Dahan[1], Gur Yaari[3], Mats Bemark[2] and Ziv Shulman[1]*

Affiliations:

[1] Department of Immunology, [4] Department of Life Science Core facilities, Weizmann Institute of Science, Rehovot, Israel.

[2] Department of Microbiology and Immunology, Institute of Biomedicine, University of Gothenburg, Sweden.

[3] Faculty of Engineering, Bar Ilan University, Ramat Gan, Israel.

* Correspondence to: ziv.shulman@weizmann.ac.il.

Abstract

Gut-derived antigens trigger immunoglobulin A (IgA) immune responses that are initiated by cognate B cells in the Peyer's patch (PP). These cells colonize the subepithelial domes (SEDs) of the PP, and subsequently infiltrate into pre-existing germinal centers (GCs). Here, we defined the pre-GC events and the microanatomical site at which affinity-based B cell selection occurred in PPs. Using whole-organ imaging, we showed that the affinity of the B cell antigen receptor (BCR) regulated infiltration of antigen-specific B cells into GCs, but not clonal competition in the SED. Follicular helper-like T cells resided in the SED and promoted its B cell colonization, independently of the magnitude of BCR affinity. Imaging and immunoglobulin sequencing indicated that selective clonal-expansion ensued during infiltration into GCs. Thus, in PPs, in contrast to draining lymph nodes and spleen, T cells predominantly promoted expansion of B cells without clonal selection during pre-GC events. These findings have major implications for the design of oral vaccines.

The initiation of an effective antibody immune response and establishment of enduring protection from invading pathogens depends on formation of long-lived plasma and memory B cells[1–3]. Generation of these cells takes place primarily in germinal centers (GCs) where B cells undergo diversification by somatic hypermutation (SHM) and affinity-based clonal selection[4–7]. These events lead to an increase in immunoglobulin affinity over time, a process known as antibody affinity maturation[2,4,8]. In draining lymph nodes (LNs) and in the spleen, antigen-specific B cells compete for GC entry at the boundary between the T cell zone and the B cell rich follicles based on the affinity of the B cell antigen receptor (BCR)[9–11]. Selection of B cells for GC seeding or for differentiation into early plasmablasts is regulated by T follicular helper cells (T_{FH} cells), which physically interact with B cells and discern high- versus low-affinity clones based on the capacity of their BCR to take up and present antigen on their surface[9,12]. However, it remained unknown whether these findings also apply to mucosal-associated lymphoid organs.

The major immunoglobulin isotype produced in intestinal tissues, IgA, is secreted by plasma cells that originate primarily from Peyer's patches (PPs), lymphoid organs that are located along the small intestine[13–15]. As opposed to LNs, which drain lymphatics and typically lack B cell activity in the absence of stimulation, PPs lack afferent lymphatic vessels and host chronically-induced and T cell-dependent GCs that are formed in response to commensal bacteria and food-derived immunogens[14,16]. Antigens are predominantly transported from the gut lumen through the follicle-associated epithelium that covers the PP by specialized epithelial cells, known as microfold (M) cells[17]. These cells transcytose luminal antigens into the subepithelial domes (SEDs) in PPs, where B

cells and antigen presenting cells reside[16,18]. CCR6 is a G-protein coupled receptor that mediates chemotactic migration of immune cells towards its ligand, CCL20[19,20]. In PPs, CCR6 plays a critical role in B cell entry into the SED, where the necessary signals for class switch recombination to the IgA isotype are provided[20,21]. Subsequently, antigen-specific B cells do not migrate towards the T cell zone[11] but rather infiltrate preformed GCs that support immune responses to different antigens[20,22]. Whether affinity-based selection takes place during the pre-GC events in the SED and the role of T cells in this process was not examined.

In the current study, we used whole-organ imaging by light sheet fluorescence microscopy (LSFM) for detection of transgenic B cells bearing high or low affinity BCRs in PPs. This technique allowed us to efficiently visualize multiple niches within intact PPs and examine the impact of BCR affinity and T cell help on B cell colonization of the SED and GC compartments. We found that effective B cell expansion in the SED predominantly depended on local delivery of T_{FH} cell-derived signals to antigen-specific B cells, independently of clonal selection.

Results

Whole-organ imaging captures all the SEDs and GCs in intact PPs

B cells interact with antigen, express activation-induced cytidine deaminase (AID) and class switch to IgA within the SED compartment[20,23]. To visualize all B cell compartments in intact PPs, we used LSFM in AID fate-reporter mice *Aicda*$^{Cre/+}$Rosa26$^{Stop\text{-}tdTomato/+}$, in which B cells express tdTomato fluorescent protein during and following AID expression[24]. LSFM imaging of intact PPs revealed GC

structures that were coupled to clusters of tdTomato^{+} B cells within the SED facing the lumen of the gut **(Fig. 1a, Supplementary Video 1)**. Expression of CCR6 on multiple cell types, is essential for proper formation and organization of the SED immune niche[20,21,23]. Accordingly, PPs derived from *Ccr6*$^{-/-}$*Aicda*$^{Cre/+}$Rosa26$^{Stop\text{-}tdTomato/+}$ hosted significantly fewer and smaller GCs compared to wild-type mice and no tdTomato^{+} B cells were detected in proximity to the lumen **(Fig. 1a-c)**, indicating that whole-organ imaging detected B cells in the SEDs.

To study the immune response of antigen-specific B cells in PPs, splenic B cell were isolated from mice that express DsRed or GFP ubiquitously and carry the *Igh*$^{B1\text{-}8hi}$ heavy chain allele that generate a BCR specific for 4-hydroxy-3-nitrophenylacetyl (NP) when coupled with Igλ light chain[25]. B1-8^{hi} DsRed^{+} Igλ^{+} B cells derived from these mice were transferred into wild-type mice prior to oral immunization. To effectively deliver a cognate oral immunogen into PPs through M cells, we used NP coupled to cholera toxin (NP-CT) as an antigen[22]. This type of oral immunization did not induce damage to the mucosal surfaces **(Supplementary Fig. 1)**. To visualize B cell immune responses in defined GC and SED niches, we imaged transferred B1-8^{hi} DsRed^{+} B cells in mice that carry an *Aicda*-transgene fused to *GFP* (AID-GFP)[24]. One day following cell transfer, AID-GFP host mice were orally immunized with NP-CT. Nine days after antigen administration, we detected B1-8^{hi} DsRed^{+} B cells among host AID-GFP^{+} B cells in the GCs and SEDs of the PP **(Fig. 1d, Supplementary Video 2)**, while almost no B1-8^{hi} DsRed^{+} B cells were detected in the PPs of mice that did not receive NP-CT **(Fig. 1d)**. Imaging of B1-8^{hi} Ccr6$^{GFP/+}$ DsRed^{+} B cells in wild-type mice immunized with NP-CT confirmed that B cells expressed CCR6 in the SED, but not in the GC **(Fig. 1e)**[20,21]. As

100 expected, transferred B1-8^{hi} DsRed^{+} B cells were found next to CD11c^{+} cells (DCs and B
101 cells) and CX3CR1^{+} macrophages in the SED **(Fig. 1f,g, Supplementary Video 3 and**
102 **4)**[16,26]. These results indicate that LSFM can be used for large-scale analysis of B cell
103 immune responses in multiple compartments within the PP.
104
105 **BCR affinity regulates B cell GC entry but not SED colonization**
106 To assess whether an affinity-based B cell selection takes place in the SED, we examined
107 the capacity of B1-8^{hi} GFP^{+} Igλ^{+} and B1-8^{lo} DsRed^{+} Igλ^{+} B cells which express BCRs
108 with a 40-fold difference in affinity for NP, to colonize different PP compartments[25]. To
109 minimize competition of transferred cells with endogenous B cells, we used MD4 host
110 mice, in which nearly all B cells (99%) are specific for hen egg lysozyme (HEL)[9,27,28].
111 MD4 mice had pre-existing GCs in their PPs that contained HEL-specific B cells without
112 prior exposure to antigen (HEL) **(Supplementary Fig. 2a)**[27]. Transferred B1-8^{hi} GFP^{+} B
113 cells had entered and expanded in the SED 4 days after NP-CT administration, and were
114 detected in the GCs by day 9 **(Fig. 2a-c, Supplementary Fig. 2b and Video 5)**. B1-8^{lo}
115 DsRed^{+} B cells expanded in the SED four days after NP-CT delivery, but were not
116 detected in the GCs at day 9 and instead accumulated in the SED **(Fig. 2a-c,**
117 **Supplementary Video 6)**. These observations indicate that the magnitude of the BCR
118 affinity regulated the infiltration of B cells into pre-existing GCs; however, B cells with
119 low affinity BCRs were able to colonize the SEDs.
120 To determine whether affinity-based competition took place in the SED, we co-
121 transferred a mixture of B1-8^{hi} GFP^{+} and B1-8^{lo} DsRed^{+} B cells at a 1:1 ratio into MD4
122 hosts, followed by NP-CT delivery. After nine days, LSFM imaging indicated that B1-8^{hi}

GFP$^+$ and B1-8^{lo} DsRed$^+$ B cells colonized the SED compartment to a similar extent, while the GC was composed entirely of B1-8^{hi} GFP$^+$ B cells **(Fig. 2b,d)**. Accordingly, flow cytometric analysis revealed that very few transferred B1-8^{lo} DsRed$^+$ B cells (less than 9 %) expressed GC markers (FAS$^+$CD38$^-$) in MD4 host mice in response to NP-CT at day 9 post-antigen delivery, whether or not B1-8^{hi} GFP$^+$ B cells were present **(Fig. 2e and Supplementary Fig. 2c)**. Thus, B cell affinity-based competition did not take place during SED colonization; however, GC infiltration and/or early GC competition depended on BCR affinity.

Next, we investigated whether BCR affinity controlled B cell proliferative capacity in the SED. Intravenous infusion of the nucleoside analog 5-ethynyl-2'-deoxyuridine (EdU) into wild-type mice followed by flow cytometry analysis revealed that CD38$^+$CCR6$^+$IgA$^+$ B cells in the SED were highly proliferative compared to CD38$^-$CCR6$^-$FAS$^+$IgA$^+$ GC B cells **(Fig. 2f and Supplementary Fig. 2d)**. We also measured EdU incorporation by transferred B1-8^{hi} GFP$^+$ and B1-8^{lo} DsRed$^+$ B cells in wild-type mice that received NP-CT orally. Flow cytometric analysis did not reveal a significant difference in EdU uptake between the two cell types **(Fig. 2g)**, indicating that BCR affinity did not dictate the magnitude of B cell proliferation in the SED.

Next, we examined whether BCR affinity plays a role in plasma cell formation within PPs. Two-photon laser scanning microscopy (TPLSM) imaging of PPs explanted from reporter mice, which carry a *YFP* transgene under the control the of *Prdm1* promoter (Blimp-1-YFP) indicated the presence of scattered YFP$^+$ plasma cells within the SED and in the interfollicular regions of the PP **(Fig. 2h and Supplementary Fig. 3a)**. To examine whether B cells have the capacity to differentiate into plasmablasts early during

the response, B1-8^{hi} Blimp-1-YFP DsRed^{+} B cells were transferred into wild-type mice, and PPs were examined five days after NP-CT administration. TPLSM analysis of intact PPs revealed individual B1-8^{hi} DsRed^{+} B cells that expressed Blimp-1-YFP in the SED compartment, as well as in the interfollicular regions **(Fig. 2h, and Supplementary Fig. 3b-c and Video 7)**. Flow cytometric analysis showed that on average 4.25 % of the transferred B1-8^{hi} Blimp-1-YFP DsRed^{+} B cells were Blimp-1-YFP^{+} five days after NP-CT administration (**Supplementary Fig. 3d)**. Flow cytometry quantification of the frequency of CD138^{+} plasma cells among transferred B1-8^{hi} GFP^{+} or B1-8^{lo} DsRed^{+} B cells showed no significant difference between the two types of transferred B cells at day 5 after NP-CT delivery **(Fig. 2i),** indicating BCR affinity did not influence plasma cell differentiation. These results indicate that in the SED, B cells rapidly proliferated and had the capacity to differentiate into early antibody forming cells; however, this process was not affected by the magnitude of their BCR affinity.

T_{FH} cells promote effective colonization of the SED and GC entry

In LNs, after engagement with antigen, B cells interact with cognate T cells and receive help signals that promote clonal selection[9,11]. To investigate the role of T cells in the SED, B1-8^{hi} GFP^{+} B cells were transferred into wild-type mice and allowed to colonize this compartment, followed by an intravenous dose of depleting antibody against CD4 five days after NP-CT delivery. LSFM analysis nine days after immunization revealed that B1-8^{hi} GFP^{+} B cells did not infiltrate the GCs and the size of the SED compartment was reduced by 1.77-fold compared to untreated wild-type mice **(Fig. 3a-c)**. To specifically examine the role of T cell help in this process, we used *Sh2d1a*$^{-/-}$ mice, which

lack expression of the SLAM-associated protein (SAP) as hosts. In these mice $CD4^+$ T cells are unable to interact with antigen-specific B cells and deliver them with help signals and as a result, the T cell-dependent antibody immune response is severely impaired[29,30]. LSFM imaging indicated that B1-8^{hi} GFP^+ B cells transferred into *Sh2d1a*$^{-/-}$ mice colonized the SED 2.85-fold less efficiently than in wild-type mice, and no GCs were formed **(Fig. 3a-c)**. These results indicate that optimal SED colonization of B cells was dependent on T cell help, while GC infiltration was strictly T cell dependent.

To examine whether B cells physically interacted with helper T cells in the SED, we performed whole-mount staining of $CD4^+$ cells within intact PPs dissected from *Aicda*$^{Cre/+}$ Rosa26$^{Stop\text{-}tdTomato/+}$ mice. Using TPLSM, $CD4^+$ T cells were detected in close contact with polyclonal $tdTomato^+$ B cells, which typically respond to food and bacterial antigens[20] **(Fig. 3d)**. Similar results were obtained by visualization of transferred B1-8^{hi} $tdTomato^+$ B cells (derived from *Igh*$^{B1\text{-}8hi}$ *Rosa26*$^{tdTomato/+}$ mice) in wild-type hosts four days after NP-CT administration **(Fig. 3d)**. These observations suggest that $CD4^+$ T cells regulated B cell functions in the SED by forming physical contacts with B cells.

To characterize the $CD4^+$ T cells in the SED, we labeled immune cells *in situ* within the SED and examined their identity by flow cytometric analysis[31,32]. For this, we generated mixed bone marrow chimeric mice in which 10% of the hematopoietic cells were derived from AID-GFP mice (used as a landmark for the SED) and 90% of the hematopoietic cells were derived from mice that express photoactivatable GFP (PA-GFP) ubiquitously **(Fig. 3e,f)**. In response to two-photon irradiation, PA-GFP shifts its excitation peak from 415nm (inactive-PA-GFP), to 495nm (active-PA-GFP); however, irradiated cells also retain the inactive-PA-GFP form[31]. Flow cytometric analysis of inactive-PA-GFP^+active-

PA-GFP$^+$ cells derived from the SED revealed that on average, 23.6 % of the local resident cells were CD4$^+$ T cells, and on average 97.1 % of the CD4$^+$ T cells were CD44$^+$CD62L$^-$ activated (CD44$^+$CD62L$^-$) T cells **(Fig. 3g-j)**. Within the CD44$^+$CD62L$^-$ CD4$^+$ T cell fraction, 27.5 % on average expressed the T_{FH} cell markers CXCR5 and PD-1, whereas naïve CD4$^+$ T cells did not express these receptors **(Fig. 3i,j)**. Similar analysis of GC T cells indicated that on average 93.5 % of the CD4$^+$ T cells in the GCs were CD44$^+$CD62L$^-$ activated T cells and on average 47.6 % of the photoactivated CD4$^+$ T cells were PD-1$^+$CXCR5$^+$ T_{FH} cells **(Supplementary Fig. 4a-d)**. The CD38$^-$FAS$^+$ GC B cells/CD44$^+$CD62L$^-$PD-1$^+$CXCR5$^+$ T_{FH} cells ratio among the photoactivated cells in the GC was similar to the ratio observed in the SED **(Supplementary Fig. 4e)**, suggesting similar availability of T_{FH} cells for a given number of B cells in the two niches. Together, these results indicate that T_{FH}-like cells resided in the SED compartment and supported B cell functions.

B cell competition for T cell help ensues during entry into GCs

In draining LNs, high and low affinity clonal variants are subjected to selective forces imposed by the limiting number of T_{FH} cells that ensue prior to GC seeding[33,34]. To examine where competition for T cell help occurs in PPs, we compared SED colonization and GC infiltration by B cells that express the same BCR, but elicit differential T cell help signals. Expression of ICAMs on B cells is not required for GC formation; however, they serve as amplifiers of T cell help signals and promote clonal selection for GC seeding[12]. Mice that express GFP ubiquitously and carry *Igh*$^{B1\text{-}8hi/+}$ were crossed to *Icam1*$^{-/-}$ and *Icam2*$^{-/-}$ mice (herein, *Icam1/2*$^{-/-}$). LSFM indicated that transferred B1-8^{hi} *Icam1/2*$^{-/-}$

GFP$^+$ B cells colonized the SED and GCs in wild-type mice to a similar extent as B1-8^{hi} *Icam1/2*$^{+/+}$ DsRed$^+$ B cells at day 9 after NP-CT immunization (**Fig. 4a,b)**. Furthermore, no significant difference in the SED colonization capacity was detected between B1-8^{hi} *Icam1/2*$^{-/-}$ GFP$^+$ B cells and B1-8^{hi} *Icam1/2*$^{+/+}$ DsRed$^+$ B cells when co-transferred (1:1 ratio) into wild-type mice and analyzed nine days after NP-CT delivery (**Fig. 4c,d)**. In contrast, the GC compartment was mainly composed of B1-8^{hi} *Icam1/2*$^{+/+}$ DsRed$^+$ B cells, 20.94-fold more than B1-8$^{hi\ +}$ *Icam1/2*$^{-/-}$ GFP B cells **(Fig. 4c,d)**. LSFM imaging revealed that transferred B1-8^{hi} *Icam1/2*$^{-/-}$ GFP$^+$ B cells were found in close proximity to the GC structure, suggesting that these cells were outcompeted after departure from the SED, during or after entry into the GC. Thus, T cell help is a limiting factor for B cell infiltration into GCs, but not for initial colonization of the SED niche.

T cell help is insufficient to promote clonal selection in SEDs

Orally delivered antigens are subjected to dilution and proteolysis along the intestinal tract. To examine if variable amounts of antigen throughout the small intestine affect SED and GC colonization, we used flow cytometry to quantify the frequency of B1-8^{hi} GFP$^+$ GC B cells in single PPs in mice, nine days after NP-CT administration. B1-8^{hi} GFP$^+$ B cells efficiently infiltrated pre-existing GCs in the duodenum PP (36 % of total GC cells), whereas this process was progressively less efficient towards the ileum PP (6.4 % of total GC cells) **(Fig. 5a)**. However, the frequency of antigen-specific CD38$^+$CCR6$^+$IgA$^+$ SED B cells in individual PPs dissected from different parts of the small intestine was roughly comparable (except the most distal PP) **(Fig. 5a)**. The differences in GC and SED colonization were not a result of differential homing of naïve

B cells to these PPs **(Supplementary Fig. 5a,b)**. Similar results were obtained in wild-type mice treated with antibiotics **(Supplementary Fig. 5c,d)**, indicating that the presence of commensal bacteria did not affect the magnitude of the GC response. As such, the amount of antigen delivered into the PP imposes a major limitation on antigen-specific B cell infiltration into the GCs, whereas colonization of the SED is less affected.

Antigen availability greatly influences the ability of cognate B cells to take up antigen and promote effective interactions with T cells[9]. DEC205 (encoded by *Ly75*) is expressed on activated B cells and mediates antigen endocytosis followed by peptide loading on MHCII molecules[31]. To determine whether antigen presentation by B cells was a limiting factor in promoting competition in the SED, we artificially loaded antigen on MHCII by using a chimeric DEC205 antibody fused to a dominant peptide derived from CT β subunit (CTB)[35]. A mixture of B1-8^{hi} *Ly75*$^{-/-}$ CD45.1^{+} and B1-8^{hi} *Ly75*$^{+/+}$ tdTomato^{+} B cells (~30:70) was transferred into wild-type mice followed by NP-CT immunization. Five days later, we intravenously injected DEC-CTB antibody or control DEC-OVA antibody or PBS into host mice and analyzed the GC and SED compartments after additional 4 days (**Supplementary Fig. 5e)**. Injection of DEC-CTB antibody increased the proportion of IgA^{+}CCR6^{+} B cells in the SED compartment by 1.55-fold compared to control treatments **(Fig. 5b,c)** suggesting that T cell help promotes B cell expansion in the SED. Next, to investigate whether selective clonal expansion takes place, we normalized the frequency of the transferred B cells to their initial frequency in the transferred mixture. B1-8^{hi} *Ly75*$^{+/+}$ tdTomato^{+} B cells were enriched 1.65-fold in the SED compared to B1-8^{hi} *Ly75*$^{-/-}$ CD45.1^{+} B cells in mice treated with DEC-CTB antibody **(Fig. 5b,d)**. In the GCs of DEC-CTB treated mice, the frequency of B1-8^{hi}

Ly75$^{+/+}$ tdTomato^{+} B cells was increased by 2.58-fold compared to B1-8^{hi} *Ly75*$^{-/-}$ CD45.1^{+} B cells **(Fig. 5e,f)**. These data demonstrate that high antigen presentation by B cells provided a selective advantage in the SED and promoted effective affinity-based infiltration and/or competition in the GC compartment.

The BCR actively signals in the SED independent of its affinity

During B cell immune responses, the BCR triggers a series of phosphorylation events essential for B cell activation[36]. Nurr77 expression (encoded by *Nr4a1*) is induced upon BCR triggering[37]. To understand whether BCR signaling in the SED played a role in BCR affinity-dependent GC infiltration, we examined PP-derived B cells from reporter mice that express GFP under *Nr4a1* transgene promoter (herein, Nurr77-GFP) by flow cytometry. CD38^{+}CCR6^{+}IgA^{+} B cells in the SED had a 5-fold higher expression of Nurr77-GFP compared to CD38^{-}FAS^{+}IgA^{+} GC B cells **(Fig. 6a)**. Flow cytometry analysis of NP-specific B cells by staining PP cells of NP-CT immunized Nurr77-GFP mice with NP-PE indicated higher Nurr77-GFP expression in CD38^{+}CCR6^{+}IgA^{+} SED B cells compared to CD38^{-}FAS^{+}IgA^{+} GC B cells **(Fig. 6b and Supplementary Fig. 5f and 6a,b)**. Furthermore, intracellular staining indicated that the B cells in the SED had higher expression of pErk and pSyk compared to GC and naïve B cells **(Fig. 6c,d)**, suggesting that the BCRs on SED B cells were actively engaged in signaling.

Next, to investigate whether the magnitude of the BCR affinity regulated the phosphorylation events within SED B cells, we transferred either B1-8^{hi} GFP^{+} or B1-8^{lo} DsRed^{+} B cells into wild-type host mice prior to NP-CT immunization. Five days later, at the time of SED colonization, intracellular staining showed no significant difference in

pErk or pSyk between B1-8^{hi} GFP^{+} or B1-8^{lo} DsRed^{+} B cells **(Fig. 6e,f)**. Thus, BCR affinity did not play a role in the magnitude of downstream activation events in the SED.

Selective clonal expansion occurs after initial SED colonization

To investigate whether our observations apply to polyclonal B cells that respond to gut-derived antigens, we examined B cell clonal variations and inter-clonal relationships in *Aicda*$^{Cre/+}$Rosa26$^{Stop\text{-}tdTomato/+}$ mice. Individual tdTomato^{+}CCR6^{+}FAS^{+}GL-7^{-}IgA^{+} SED B cells and tdTomato^{+}CCR6^{-}FAS^{+}GL-7^{+}IgA^{+} GC B cells were sorted from a single PP and subjected to *Igh* mRNA sequencing and CDR3-based clustering **(Supplementary Fig. 6c)**. We found limited V segment usage in the GC B cells, and nearly all the cells were clonally expanded (90 % on average) **(Fig. 7a,b)**. Conversely, V segment usage was highly diverse in SED B cells and fewer clones were detected more than once (38 % on average) **(Fig. 7b,c)**. These results suggest that clonal selection for extensive expansion and GC seeding took place after initial SED colonization.

Class-switched B cells were shown to depart the SED and infiltrate GCs[20,24]. Accordingly, we observed that an average of 7 % of IgA^{+} clones in the SED were also represented in the GC compartment; however, half of the highly-expanded clones (>5 clonal members) were present in both compartments **(Fig. 7b,c)**. Comparison of SHM indicated that GC B cells had more mutations in the *Igh* genes than SED B cells **(Fig. 7d)**. Clones detected in both compartments had a similar number of SHM in the *Igh* transcript, while non-shared clones derived from the SED compartment carried 2.4-fold fewer mutations compared to the shared clones **(Fig. 7e)**. These results suggest that highly mutated clones in the SED originated from the GC.

To gain additional insight into the clonal relationships in PPs, we constructed evolutionary phylogenetic trees of the B cell clones found in both compartments. We found several clonal families in which clonal members in the SED compartment had generated highly diversified descendants in the GCs **(Fig. 7f and Supplementary Fig. 7**). In addition, we found highly-diversified clones within the GC compartment that had generated clonal members in the SED compartment **(Fig. 7f)**. These observations indicate that diversified IgA^+ GC B cells re-entered the SED compartment as mutated GC-derived memory B cells.

Discussion

In the PPs, activated B cells occupy two major niches, the SED, located under the follicle-associated epithelium, and the GC structures, positioned distal to the gut lumen within the B cell follicles[16]. Here, we identified the site at which affinity-based B cell selection was initiated in PPs and define the role of BCR affinity in regulating B cell responses. We found that several processes that regulate pre-GC events in the SED differed from those that occur in the draining LN and spleen: in the PP, antigen-specific B cells were not subjected to affinity-based competition in the SED prior to GC entry; T cells predominantly promoted B cell expansion without clonal selection at the pre-GC stage; B cell affinity-based competition ensued during or immediately after GC infiltration; and GC-derived memory cells and plasmablasts were found in the SED.

The nature of the intestinal environment, as well as the requirement for active transport of luminal antigens into the PPs, greatly affect the amount of antigen available for triggering a cognate B cell immune response[15]. In germ free mice the IgA response is triggered only

330 when a large dose of commensal bacteria is administered[38], indicating that a large amount
331 of antigen is required for delivery of antigens into the PPs and/or initiation of the GC
332 response. In support of these observations, we demonstrated that both BCR affinity and
333 antigen availability promoted effective infiltration into the GC structures. In sharp
334 contrast, the magnitude of B cell activation dictated by these two factors had only a small
335 impact on initial BCR signaling, as well as proliferation in the SED, once a minimal
336 threshold was reached. This suggests that in PPs the threshold for GC entry is higher than
337 the threshold that triggers BCR signaling and B cell proliferation in the SED. The GCs
338 contain follicular dendritic cells (FDC) that reside in the light zone and capture antigens
339 on their surface and present it to B cells[39]. These cells have the capacity to augment
340 effective BCR triggering by increasing antigen density on their surface using receptors
341 that capture antibody-antigen complexes[39]. Generation of plasmablats early during the
342 response in the SED and interfollicular regions of the PPs, could potentially provide
343 antibodies that complex with cognate antigens on FDCs and support effective clonal
344 competition in the GCs over an extended period of time, even when antigen levels are
345 extremely low.
346 T_{FH} cells play an important role in regulating the B cell response in the SED without
347 promoting affinity-based clonal selection, most likely through CD40 ligation on B cells[20].
348 The inability of T cells to promote clonal selection in the PP SED indicates that TCR
349 binding of peptide-loaded MHCII (pMHCII) on B cells are not sufficient to support this
350 process. Artificial increase of antigen presentation on B cells endowed them with a
351 selective advantage, suggesting that in response to vaccination, the density of pMHCII
352 was too low to promote clonal selection. We suggest that there are two different T cell

help thresholds in PPs: one for maintaining B cells in the SED, and one for promoting clonal selection, which depends on higher surface presentation of pMHCII. Clonal selection in the SED might take place when cognate antigen levels in the gut are extremely high, such as during breach of the gut epithelium and invasion of commensal or pathogenic bacteria into the host tissues.

Consistent with T_{FH} cell functions, we found that SAP-dependent T cell help promoted B cell SED colonization. Nonetheless, although T cells and CD40 signaling play an important role in entry into the SED[20], antigen-specific B cells could access this compartment, independently of effective T cell help. BCR engagement is sufficient for CCR6 expression[20,40,41], suggesting that B cells that encounter antigen can gain access to the SED niche independently of T cell functions. Indeed, we found that B cells in the SED were constantly engaged in signaling, independently of the BCR affinity. This indicates that signals derived from T_{FH}-like cells synergize with BCR signals to promote entry and/or non-selective expansion of antigen-specific B cells in the SED.

The major purpose of the GC is to produce long-lived memory and plasma cells that produce protective high-affinity antibodies[14]. We identified highly-mutated $CCR6^{+}IgA^{+}$ B cells that typically reside in the SED and provided evidence for the presence of GC-derived memory B cells at this site; whether these cells directly migrate from the GC to the SED or first enter the circulation is yet to be determined[42,43].

Collectively, we found that the SED niche was important for the initial expansion of B cells bearing high- and low-affinity BCRs, followed by competitive GC infiltration into preformed GC structures. These findings have far ranging implications in oral vaccine

design for the generation of memory GC-derived IgA^+ B cells with high-affinity BCRs specific for intestinal pathogens.

Accession code: PRJEB30525.

Acknowledgments: Z.S. is supported by the European Research Council (ERC) grant No. 677713, Human Frontiers of Science Program (CDA-00023/2016), Israel Science Foundation (ISF) grant no. 1090/18, Azrieli Foundation, Rising Tide Foundation, and the Morris Kahn Institute for Human Immunology. Z.S. is a member in the European Molecular Biology Organization (EMBO) Young Investigator Program and is supported by grants from The Benoziyo Endowment Fund for the Advancement of Science, The Sir Charles Clore Research Prize, Comisaroff Family Trust, Irma & Jacques Ber-Lehmsdorf Foundation, Gerald O. Mann Charitable Foundation and David M. Polen Charitable Trust. Imaging was made possible thanks to the "The de Picciotto-Lesser Cell Observatory in memory of Wolf and Ruth Lesser".

Author contributions: A.B. designed and conducted the experiments, performed data analysis and wrote the manuscript; A.S. prepared the in-house antigen used in this study; E.W. analyzed single-cell immunoglobulin sequencing data; L.S.B. and Y.A. assisted with light sheet imaging; R.S. and R.D. produced antibodies used in this study. G.Y. supervised immunoglobulin-sequencing analysis; M.B. advised and helped in the design of some of the experiments; and Z.S. designed experiments, supervised the study and wrote the manuscript.

Competing interests: The authors declare no competing interests.

References

1. De Silva, N. S. & Klein, U. Dynamics of B cells in germinal centres. *Nat. Rev. Immunol.* **15,** 137–148 (2015).
2. Victora, G. D. & Nussenzweig, M. C. Germinal Centers. *Annu. Rev. Immunol.* **30,** 429–457 (2012).
3. Allen, C. D. C., Okada, T. & Cyster, J. G. Germinal-Center Organization and Cellular Dynamics. *Immunity* **27,** 190–202 (2007).
4. Eisen, H. N. & Siskind, G. W. Variations in Affinities of Antibodies during the Immune Response. *Biochemistry* **3,** 996–1008 (1964).
5. Berek, C., Berger, A. & Apel, M. Maturation of the immune response in germinal centers. *Cell* **67,** 1121–1129 (1991).
6. Jacob, J., Kelsoe, G., Klaus, R. & Weiss, U. Interclonal generation of antibody mutants in germinal centres. *Lett. to Nat.* **353,** 389–392 (1991).
7. Rajewsky, K. Clonal selection and learning in the antibody system. *Nature* **381,** 751–758 (1996).
8. Goidl, E. A., Paul, W. E., Siskind, G. W., Benacerraf, B. & Kelsoe, G. The effect of antigen dose and time after immunization on the amount and affinity of anti-hapten antibody. *J. Immunol.* **100,** 371–5 (1968).
9. Schwickert, T. A. *et al.* A dynamic T cell–limited checkpoint regulates affinity-dependent B cell entry into the germinal center. *J. Exp. Med.* **208,** 1243–1252 (2011).
10. Abbott, R. K. *et al.* Precursor Frequency and Affinity Determine B Cell Competitive Fitness in Germinal Centers, Tested with Germline-Targeting HIV

Vaccine Immunogens. *Immunity* **48,** 133–146.e6 (2018).

11. Okada, T. *et al.* Antigen-engaged B cells undergo chemotaxis toward the T zone and form motile conjugates with helper T cells. *PLoS Biol.* **3,** 1047–1061 (2005).

12. Zaretsky, I. *et al.* ICAMs support B cell interactions with T follicular helper cells and promote clonal selection. *J. Exp. Med.* **214,** jem.20171129 (2017).

13. Craig, S. W. & Cebra, J. J. Peyer's patches: an enriched source of precursors for IgA-producing immunocytes in the rabbit. *J. Exp. Med.* **134,** 188–200 (1971).

14. Pabst, O. New concepts in the generation and functions of IgA. *Nat. Rev. Immunol.* **12,** 821–832 (2012).

15. Macpherson, A. J., Geuking, M. B., Slack, E., Hapfelmeier, S. & McCoy, K. D. The habitat, double life, citizenship, and forgetfulness of IgA. *Immunol. Rev.* **245,** 132–46 (2012).

16. Reboldi, A. & Cyster, J. G. Peyer's patches: Organizing B-cell responses at the intestinal frontier. *Immunol. Rev.* **271,** 230–245 (2016).

17. Neutra, M. R., Mantis, N. J. & Kraehenbuhl, J. P. Collaboration of epithelial cells with organized mucosal lymphoid tissues. *Nat. Immunol.* **2,** 1004–1009 (2001).

18. Lycke, N. Y. & Bemark, M. The regulation of gut mucosal IgA B-cell responses: Recent developments. *Mucosal Immunol.* **10,** 1361–1374 (2017).

19. Elgueta, R. *et al.* CCR6-Dependent Positioning of Memory B Cells Is Essential for Their Ability To Mount a Recall Response to Antigen. *J. Immunol.* **194,** 505–513 (2015).

20. Reboldi, A. *et al.* IgA production requires B cell interaction with subepithelial dendritic cells in Peyer's patches. *Science.* **352,** aaf4822 (2016).

21. Lin, Y. L., Ip, P. P. & Liao, F. CCR6 deficiency impairs IgA production and dysregulates antimicrobial peptide production, altering the intestinal flora. *Front. Immunol.* **8,** 1–20 (2017).

22. Bergqvist, P. *et al.* Re-utilization of germinal centers in multiple Peyer's patches results in highly synchronized, oligoclonal, and affinity-matured gut IgA responses. *Mucosal Immunol.* **6,** 122–135 (2013).

23. Cook, D. N. *et al.* CCR6 mediates dendritic cell localization, lymphocyte homeostasis, and immune responses in mucosal tissue. *Immunity* **12,** 495–503 (2000).

24. Rommel, P. C. *et al.* Fate mapping for activation-induced cytidine deaminase (AID) marks non-lymphoid cells during mouse development. *PLoS One* **8,** e69208 (2013).

25. Shih, T. A. Y., Meffre, E., Roederer, M. & Nussenzweig, M. C. Role of BCR affinity in T cell-dependent antibody responses in vivo. *Nat. Immunol.* **3,** 570–575 (2002).

26. Wagner, C. *et al.* Some news from the unknown soldier, the Peyer's patch macrophage. *Cell. Immunol.* (2018). doi:10.1016/j.cellimm.2018.01.012

27. Casola, S. *et al.* B cell receptor signal strength determines B cell fate. *Nat. Immunol.* **5,** 317–327 (2004).

28. Goodnow, C. C. Balancing immunity and tolerance: deleting and tuning lymphocyte repertoires. *Proc. Natl. Acad. Sci.* **93,** 2264–2271 (1996).

29. Qi, H., Cannons, J. L., Klauschen, F., Schwartzberg, P. L. & Germain, R. N. SAP-controlled T?B cell interactions underlie germinal centre formation. *Nature* **455,**

764–769 (2008).

30. Crotty, S., Kersh, E. N., Cannons, J., Schwartzberg, P. L. & Ahmed, R. SAP is required for generating long-term humoral immunity. *Nature* **421,** 282–7 (2003).

31. Victora, G. D. *et al.* Germinal center dynamics revealed by multiphoton microscopy with a photoactivatable fluorescent reporter. *Cell* **143,** 592–605 (2010).

32. Medaglia, C. *et al.* Spatial reconstruction of immune niches by combining photoactivatable reporters and scRNA-seq. *Science (80-.).* **358,** 1622–1626 (2017).

33. Kuraoka, M. *et al.* Complex Antigens Drive Permissive Clonal Selection in Germinal Centers. *Immunity* **44,** 542–552 (2016).

34. Tas, J. *et al.* Visualizing antibody affinity maturation in germinal centers. *Science.* **351,** 1048–1054 (2016).

35. Cong, Y., Bowdon, H. R. & Elson, C. O. Identification of an immunodominant T cell epitope on cholera toxin. *Eur. J. Immunol.* **26,** 2587–2594 (1996).

36. Kurosaki, T. Regulation of BCR signaling. *Mol. Immunol.* **48,** 1287–1291 (2011).

37. Mueller, J., Matloubian, M. & Zikherman, J. Cutting Edge: An In Vivo Reporter Reveals Active B Cell Receptor Signaling in the Germinal Center. *J. Immunol.* **194,** 2993–2997 (2015).

38. Hapfelmeier, S. *et al.* Reversible microbial colonization of germ-free mice reveals the dynamics of IgA immune responses. *Science* **328,** 1705–9 (2010).

39. Heesters, B. A., Myers, R. C. & Carroll, M. C. Follicular dendritic cells: Dynamic antigen libraries. *Nat. Rev. Immunol.* **14,** 495–504 (2014).

40. Wiede, F. *et al.* CCR6 is transiently upregulated on B cells after activation and modulates the germinal center reaction in the mouse. *Immunol. Cell Biol.* **91,** 335–339 (2013).

41. Reimer, D. *et al.* Early CCR6 expression on B cells modulates germinal centre kinetics and efficient antibody responses. *Immunol. Cell Biol.* **95,** 33–41 (2017).

42. Lindner, C. *et al.* Diversification of memory B cells drives the continuous adaptation of secretory antibodies to gut microbiota. *Nat. Immunol.* **16,** 880–888 (2015).

43. Bemark, M. *et al.* Limited clonal relatedness between gut IgA plasma cells and memory B cells after oral immunization. *Nat. Commun.* **7,** 1–15 (2016).

Figure Legends

Figure 1. Visualization of SED niches and GC compartments in intact Peyer's patches using light sheet fluorescence microscopy. a, Schematic representations of PP positions (upper panels). Middle and lower panels, show GCs and SEDs in a PP of *Aicda*$^{Cre/+}$Rosa26$^{Stop\text{-}tdTomato/+}$ *Ccr6*$^{+/+}$ or *Ccr6*$^{-/-}$ mice. Arrows indicate SED structures. Scale bars, 300 μm and 200 μm respectively. **b,c,** Quantification of the number (b), and volume (c) of GCs and SEDs of *Ccr6*$^{+/+}$ and *Ccr6*$^{-/-}$ mice. Each dot represents an individual PP in (b) or individual GC or SED in (c). Imaging analyses were performed in two independent experiments with a total of four mice per group (n=4), including 11 *Ccr6*$^{+/+}$ and 17 *Ccr6*$^{-/-}$ PPs, line represents mean. *** P<0.0001, two tailed Student's t test. **d,** B1-8^{hi} DsRed^{+} B cells (red) in a PP of an AID-GFP (green) mouse without antigen administration, or nine days after NP-CT administration. Scale bar, 300 μm. **e,** B1-8^{hi} Ccr6$^{GFP/+}$ DsRed^{+} B cells transferred into a WT host, nine days after oral antigen administration. Scale bar, 300μm. **f,g,** B1-8^{hi} DsRed^{+} B cells (red) in a PP of CD11c-YFP or Cx3cr1$^{GFP/+}$ reporter mice, nine days after antigen administration. The SED area is marked with a dashed line. Scale bar, 300 μm. In d-g, representative images of two independent experiments with three mice in each experiment (n=6) are shown.

Figure 2. BCR affinity controls GC infiltration but not proliferation nor early plasmablast formation in the SED. a,b, Images showing transferred B1-8^{hi} GFP^{+}, B1-8^{lo} DsRed^{+} B cells or a mixture in MD4 hosts, 4 (a), or 9 days (b) after NP-CT immunization. Scale bar, 300 μm. **c,** Quantification of SED and GC volumes. Each dot represents one compartment. Analyses were performed in two independent experiments with a total of four mice per group (n=4), including 17 B1-8^{hi} GFP^{+} and 26 B1-8^{lo}

DsRed^{+} GCs and coupled SEDs at day 4 and 19 and 36 at day 9, respectively. Line represents mean. **d,** Quantification of SED and GC volumes in MD4 mice that received a 1:1 mixture of B1-8^{hi} GFP^{+} and B1-8^{lo} DsRed^{+} B cells. Data are pooled from two independent experiments using a total of 12 compartments from three mice (n=3). Line represents mean. **e,** Flow cytometry analysis of transferred cells as in b-d. Gating is depicted in Supplementary Fig. 2d. Data are pooled from two independent experiments with a total of five or six mice per group with (n=5) and without competition (n=6), respectively, line represents mean. **f,g,** Proliferation analysis of endogenous naïve, GC and SED B cells, 2.5 hours following EdU administration (f) or in transferred B1-8^{hi} GFP^{+} and B1-8^{lo} DsRed^{+} B cells, nine days after NP-CT immunization (g). Gating strategy and additional details are described in Supplementary Fig. 2e. Data are pooled from two independent experiments with six mice per group (n=12) (f) or with three mice per group (n=6) (g), line represents mean. **h,** Blimp-1-YFP cells in the SED (left) or transferred B1-8^{hi} Blimp-1-YFP DsRed^{+} cells in the SED, five days after immunization (right). Arrowheads indicate Blimp-1-expressing cells. Scale bar, 100 μm. Images represent two independent experiments with two mice in each experiment. **i,** Analysis of CD138^{+} cells gated on B1-8^{hi} tdTomato^{+} or B1-8^{lo} DsRed^{+} B cells, five days after immunization. Line represents mean. ** P<0.01, *** P<0.0001, one-way ANOVA with Bonferroni posttest in (c) and (f), and two-tailed Student's t test in (d,e,g,i). ns, not significant.

Figure 3. Effective SED colonization by antigen-specific B cells depends on T_{FH}-like cells. a, Images of transferred B1-8^{hi} GFP^{+} B cells in WT, *Sh2d1a*$^{-/-}$, and αCD4-treated mice (days 5 and 7), nine days after NP-CT immunization. Scale bar, 300 μm.

Representative images from three experiments showed similar results. **b,c,** Volume quantification of SEDs (b), and GCs (c). Data are pooled from two independent experiments with three mice in each experiment (n=6) with 35 (WT), 28 (αCD4) and 19 (*Sh2d1a*$^{-/-}$) GCs and coupled SEDs, line represents mean. *** P<0.0001, one-way ANOVA with Bonferroni posttest. **d,** Upper panels: SED of *Aicda*$^{Cre/+}$Rosa26$^{Stop\text{-}tdTomato/+}$ mouse stained for CD4. Lower panels: B1-8^{hi} tdTomato^{+} B cells in the SED, four days after NP-CT immunization. Scale bar, 100 μm and 30 μm in zoom in images. Two independent experiments with two mice in each experiment (n=4) showed similar results. **e,** SED of AID-GFP:PA-GFP (10:90) chimeric mouse prior to and after photoactivation. Scale bar, 100 μm. **f,** Flow cytometry analyses of inactive- and active-PA-GFP cells. **g,** CD4^{+} cell frequency among the active-PA-GFP cells. **h,** Merged plot of CD4^{+}CD44^{+}CD62L^{-} cells among total CD4^{+} cells (black) and active-PA-GFP^{+}CD4^{+} cells (green). **i,** Plots showing PD-1^{hi}CXCR5^{hi} cells in the active-PA-GFP^{+}CD4^{+}CD44^{+}CD62L^{-} compartment. Lack of markers on naïve cells is shown as control. **j,** T cell frequencies are summarized in the graph as mean; each dot represents a mouse, bar represents mean. In f-j, data are pooled from three independent experiments using a total of four mice (n=4).

Figure 4. Competition for T cell help takes place during infiltration into pre-existing GC sites. a, Representative images of B1-8^{hi} *Icam1/2*$^{+/+}$ DsRed^{+} or B1-8^{hi} *Icam1/2*$^{-/-}$ GFP^{+} B cells transferred separately into WT hosts, nine days following oral antigen administration. **b,** Volumetric quantification of B cells in the SEDs and GCs of WT mice PPs under noncompetitive conditions. Data are pooled from two independent experiments with three mice in each experiment (n=6) and two PPs from each mouse, corresponding

to 36 GC and coupled SED structures. Line represents mean. Scale bar 300 μm. **c,** Representative images of B1-8^{hi} *Icam1/2*$^{+/+}$ DsRed^{+} or B1-8^{hi} *Icam1/2*$^{-/-}$ GFP^{+} B cells co-transferred at a 1:1 ratio into WT hosts, nine days following oral NP-CT immunization. A single PP (upper panels) and a single GC (lower panels) are shown. **d,** Volumetric quantification of B cells in SEDs and GCs of WT PPs transferred with cells as in (c). Data are pooled from two independent experiments with a total of seven mice (n=7), two PPs from each mouse and 56 GC and coupled SED structures, line represents mean. Scale bar, 300 μm. *** P<0.0001, two-tailed Student's t test. ns, not significant.

Figure 5. Antigen presentation by B cells in the SED is insufficient for promoting competition for T cell help. a, Frequency of B1-8^{hi} GFP^{+} B cells in GCs (FAS^{+}CD38^{-}) or SEDs (IgA^{+}CD38^{+}CCR6^{+}) of individual PPs. Data are pooled from two independent experiments with single PPs taken from two mice in each experiment (n=4). Each dot represents mean of cell frequency; error bars indicate s.e.m. **b,** Flow cytometry plots of transferred B1-8^{hi} *Ly75*$^{+/+}$ tdTomato^{+} and B1-8^{hi} *Ly75*$^{-/-}$ CD45.1^{+} B cells in the SED of immunized mice following intravenous injection of 50μg DEC205-CTB or DEC205-OVA antibodies or PBS as control, as described in Supplementary Fig. 5a. **c,** Frequencies of SED B cells following treatment with DEC205-CTB Ab or control, line represents mean. Each dot represents a single mouse. **d,** Flow cytometric analysis of transferred B1-8^{hi} *Ly75*$^{+/+}$ tdTomato^{+} and B1-8^{hi} *Ly75*$^{-/-}$ CD45.1^{+} B cells as in b, normalized to the initial percentage of the transferred cells. Line represents mean. **e,f,** Flow cytometry plots (e) and quantification of transferred cells within the GC (f) following immunization and Ab treatment, as in (b). Each B cell subset in the GC was normalized to the percentage of the transferred cells. Data shown in c-f are pooled from two independent experiments with

three mice per experiment (n=6). Each dot represents an individual mouse, line represents mean. * P<0.05, *** P<0.0001, two-tailed Student's t test in (c) and one-way ANOVA with Bonferroni posttest in (d) and (f). ns, not significant.

Figure 6. Active BCR signaling in the SED is independent of its affinity. a, Representative histogram showing Nurr77 expression in SED ($IgA^+CD38^+CCR6^+$) and GC (FAS^+CD38^-) B cells of Nurr77-GFP reporter mice. Geometric mean fluorescence intensity (gMFI) is summarized in the graph. Data are pooled from two independent experiments with three mice in each experiment (n=6), each dot represents a mouse; line represents mean. **b,** Nurr77 expression as in (a) within NP specific B cells detected using NP-PE (Supplementary Fig. 5f), 9 days after NP-CT administration. Data are pooled from two independent experiments with three mice in each experiment (n=6), each dot represents a mouse; line represents mean. *** P<0.0001, two-tailed Student's t test. **c,d,** Representative histograms showing pErk (c) or pSyk (d) in naïve, SED and GC B cells in WT mice. gMFI values are summarized in the graph. Data are pooled from two independent experiments with four mice in each experiment (n=8), each dot represents a mouse; line represents mean. ** P<0.01, *** P<0.0001, one-way ANOVA with Bonferroni posttest. ns, not significant. **e,f,** Representative histograms showing pErk (e) or pSyk (f) expression in B1-8^{hi} GFP^+ or B1-8^{lo} $DsRed^+$ B cells, 5 days after NP-CT administration. Naïve cell population expression is shown as negative control. gMFI values are summarized in the graph. Data are pooled from two independent experiments with three mice in each experiment (n=6), line represents mean. ns, not significant; two-tailed Student's t test.

Figure 7. Selective clonal expansion and diversification takes place in the GCs, but not in the SED compartment. **a,** The number of V regions detected in IgA sequences of GC or SED-derived B cells recovered from a single PP explanted from *Aicda*$^{Cre/+}$Rosa26$^{Stop\text{-}tdTomato/+}$ mice. Data are pooled from two independent experiments with one mouse per experiment (n=2), bar represents mean. **b,** Clonal distribution based on CDR3 sequences as in (a). Colored fractions represent expanded CDR3 sequences (>2), white fraction represents single clones. Each graph represents one mouse (n=2). The number of sequenced cells is indicated in the center circle. **c,** The number of clonal members detected in the GC and SED, each bar represents a clone. **d,** Number of mutations per B cell in the GC and SED. Each dot represents a cell and 183 SED and 174 GC cells are shown; line represents mean. *** P<0.0001, two-tailed Student's t test. **e,** The mutation ratio of SED and GC clones that were either unique or shared between the niches, each dot represents a mouse (n=2), bar represents mean. **f,** Lineage-tree analysis of clonally related sequences. The number of mutations between neighboring nodes is indicated and includes synonymous, non-synonymous, and reverse mutations to the germline sequence. GL, germline. UCA, unique common ancestor, inferred from the sequence analysis. Additional linage-trees are available in Supplementary Fig. 7. Data are pooled from two independent experiments with one mouse per experiment.

Methods

Mice

Transgenic knock-in mice carrying the *Igh*$^{B1\text{-}8hi}$ or *Igh*$^{B1\text{-}8lo}$ alleles[25] or *Ly75*$^{-/-}$ mice were a gift of M. Nussenzweig (The Rockefeller University). AID-GFP mice were generated by R. Casellas (NIAMS, NIH) and provided by M. Nussenzweig. GFP-, DsRed-, PA-GFP-expressing mice and MD4, *Aicda*^{Cre}, Rosa26$^{Stop\text{-}tdTomato}$, *Sh2d1a*$^{-/-}$ [30], Blimp-1-YFP, Nurr-77-GFP and Ccr6$^{GFP/+}$ mice were purchased from the Jackson Laboratories. GFP- and DsRed-expressing mice were bred to mice that carry either the *Igh*$^{B1\text{-}8hi}$ or *Igh*$^{B1\text{-}8lo}$ alleles[25]. tdTomato^{+} mice were generated by crossing Rosa26$^{Stop\text{-}tdTomato}$ mice to a Cre expressing strain. *Icam1/2*$^{-/-}$ mice were provided by B. Engelhardt (University of Bern) and bred with *Igh*$^{B1\text{-}8hi}$ GFP-expressing mice. *Ly75*$^{-/-}$ mice were crossed with mice carrying the *Igh*$^{B1\text{-}8hi}$ and the congenic marker CD45.1 to produce *Igh*$^{B1\text{-}8hi}$ *Ly75*$^{-/-}$ CD45.1-expressing mice. CD11c-YFP and Cx3cr1$^{GFP/+}$ mice were provided by S. Jung (Weizmann Institute). Wild-type mice (C57BL/6) were purchased from Harlan. All experiments with mice were approved by the Weizmann Institute Animal Care and Use Committee (IACUC).

Adoptive cell transfer

B cells were purified by forcing spleen tissue through mesh into PBS containing 2% fetal calf serum and 1 mM EDTA. Resting B cells were purified using negative selection anti-CD43 magnetic beads (Miltenyi Biotec). For Igλ B cell purification, cells were incubated with anti- Igκ-PE antibody for 30 min at 4^{o}C. Cells were washed, and Igκ B cells were depleted using anti-PE magnetic beads (Miltenyi Biotec.). Igλ enrichment was verified by flow cytometry prior to cell transfer. Isolated cells (100K, Igλ) were injected

intravenously into host mice one day before oral antigen administration. In competition experiments, the ratio of adoptively transferred cells (B1-8^{hi} GFP^{+} and B1-8^{lo} DsRed^{+} B cells or B1-8^{hi} *Icam1/2*$^{+/+}$ DsRed^{+} and B1-8^{hi} *Icam1/2*$^{-/-}$ GFP^{+} B cells) was 1:1 (1x10^{5} of each cell type). In experiments involving transfer of B1-8^{hi} *Ly75*$^{-/-}$ CD45.1^{+} and B1-8^{hi} *Ly75*$^{+/+}$ tdTomato^{+} B cells, the ratio was either 3:7 or 1:1 and confirmed by flow cytometer analysis of the cell mixture prior to injection of the cells into the mice. Cell frequencies (% of cells in the GC and SED compartments) were normalized to the initial cell transfer ratio.

Chimeric mice

For generation of chimeric mice, hosts were irradiated with 950 rad followed by injection of fresh BM cells. For generating chimeric mice for photoactivation experiments CD45.2^{+} hosts were reconstituted with a mixture of BM cells containing 90% BM cells derived from PA-GFP-expressing mice, and 10% BM cells derived from AID-GFP reporter mice. Chimeric mice experiments were performed 8 weeks following bone marrow transplantation.

Oral antigen administration and treatments

NP was conjugated to CT as previously described[22]. Mice received a single administration of 500µl PBS containing 3% $NaHCO_3$ and 10µg NP-CT by gavage. For CD4^{+} T cell depletion experiments, 200 µg of rat anti-mouse CD4 mAb (clone GK1.5, rIgG2b, BioXcell) was injected intravenously on days 5 and 7 following oral delivery of NP-CT. For antibiotic treatment, mice were given a combination of ampicillin (1g/l), vancomycin (0.5 g/l), neomycin sulfate (1 g/l), imipenem (250mg/l), and metronidazole

(1 g/l) (Sigma Aldrich) in their drinking water for two weeks[44]. Mice were 5 weeks of age at the beginning of antibiotic administration.

Anti-DEC205 treatment

For DEC-CTB cloning, the sequence of CTB peptide 81-100 was inserted into the DEC205 vector[35]. DEC-CTB and DEC-OVA antibodies were produced as chimeric antibodies in 293T cell as previously described[45]. Mice received 50μg of antibodies intravenously 5 days after oral antigen administration.

In vivo EdU proliferation assay

For proliferation measurements, mice were injected intravenously with 2mg of the nucleoside analog 5-ethynyl-2'-deoxyuridine (EdU) (Molecular Probes) in PBS. After 2.5 hours, mice were dissected and PP cells were then stained for surface antigens as described, followed by EdU detection using Click-iT EdU Alexa Fluor 647 Flow Cytometry Assay Kit (Molecular Probes) according to manufacturer's protocol.

Flow cytometry

Small intestines were excised and washed with ice cold PBS to remove fecal content. Peyer's patches were harvested and forced through a mesh into PBS containing 2% fetal calf serum and 1 mM EDTA. For blockade of Fc receptors, single cell suspensions were incubated with 2 μg/ml anti-16/32 (clone 93) for 5 min. Cells were washed and incubated with fluorescently labeled antibodies (Table S1) for 30 min. GC cells were gated as live/single, $B220^{+}CD38^{-}FAS^{+}$ or $B220^{+}GL\text{-}7^{+}FAS^{+}$. SED B cells were gated as $B220^{+}CD38^{hi}GL\text{-}7^{-}FAS^{+}CCR6^{+}$. Transferred cells within GCs were detected by staining cell suspensions with GC markers, as indicated, along with the endogenous fluorescent markers used for B1-8^{hi} and B1-8^{lo} B cell detection (GFP^{+}, tdTomato and $DsRed^{+}$,

707 respectively). In photoactivation experiments, T_{FH} cells were gated as
708 $CD4^+CD44^+CD62L^-$ $PD\text{-}1^+CXCR5^+$ out of the photoactivated cells or out of total
709 inactive PA-GFP cells. PA-GFP fluorescence was measured using the V500 (inactive
710 PA-GFP) and FITC (active PA-GFP) channels. In BCR signaling experiments, B1-8
711 $DsRed^+$ B cells were transferred into CD45.1 hosts and gated as $B220^+DsRed^+CD45.2^+$.
712 Intracellular staining for pErk and pSyk was performed using Foxp3 / Transcription
713 Factor Staining Buffer Set (eBioscience) according to the manufacturer's instructions.
714 Stained cell suspensions were analyzed using a CytoFlex flow cytometer (Beckman
715 Coulter).

716 **Tissue processing and image acquisition by LSFM**

717 Peyer's patches were excised and fixed in 4% PFA for 2 hours, followed by immersion in
718 FocusClear (CelExplorer Labs) for 1-4 days. Samples were imaged using a light sheet Z1
719 microscope (Zeiss Ltd.) equipped with two sCMOS PCO- Edge cameras, 10X
720 illumination objectives (LSFM clearing 10X/0.2), Clr Plan- Neofluar 20X/1,0
721 Corr nd=1.45, and detection objective designed for cleared samples in water-based
722 solution with a final refractive index (RI) of 1.45. Samples were loaded into a glass
723 capillary in a 1.5% low melting agarose solution (ROTH). Imaging was performed using
724 dual side illumination, with zoom 0.36 and multi view mode for tiling of multiple fields
725 of view, with overlap of 10%. GFP Excitation 488, Emission / detection - BP 505-545;
726 YFP Excitation 514, Emission / detection - BP 525-565; RFP Excitation 561, Emission /
727 detection - BP 575-615.

728 **Gut permeability assay**

Gut permeability assay was performed by evaluation of FITC dextran (Sigma Aldrich) in the blood as previously described[46]. WT mice received NP-CT by gavage or 3% $NaHCO_3$ as control. Gut permeability was assessed 24 hours after oral NP-CT administration. In addition, sera of mice that did not receive NP-CT and treated with FITC dextran were used as a negative control. For histological H&E analysis, mice received NP-CT orally and tissue dissection was performed 1, 5 or 9 days after NP-CT administration.

Whole mount staining

PPs of *Aicda*$^{Cre/+}$Rosa26$^{Stop\text{-}tdTomato}$ or WT cells transferred with B1-8^{hi} tdTomato^{+} B cells were harvested as described, and stained with CD4 antibody conjugated to Alexa fluor 488 (1:100) (GK1.5, Biolegend) as previously described[47]. Images were acquired by TPLSM.

Photoactivation and image acquisition by TPLSM

Zeiss LSM 880 upright microscope fitted with Coherent Chameleon Vision laser was used for photoactivation and CD4 visualization imaging experiments. Images were acquired with a femtosecond-pulsed two-photon laser tuned to 940 nm. The microscope was fitted with a filter cube containing 565 LPXR to split the emission to a PMT detector (with a 579-631 nm filter for tdTomato fluorescence) and to an additional 505 LPXR mirror to further split the emission to 2 GaAsp detectors (with a 500-550nm filter for GFP fluorescence). PPs of chimeric mice were dissected, and photoactivation of the region of interest was provided at 830 nm as previously described[31,48]. Tile images were acquired as a 100 μm Z-stacks with 5 μm steps between each Z-plane. The zoom was set to 0.7, and pictures were acquired at 512 x 512 x-y resolution.

Image analysis

LSFM image dual side fusion was performed using ZEN software. The independent tiles were stitched into a single image stack visualized in a volumetric mode using Arivis Vision4D software. Quantification of B cells in GCs and SEDs size was performed using Imaris software (Bitplane). Each compartment was segmented using the Imaris 3D surface object. Samples with clear separation between SED and GCs were segmented together. Under some conditions, in which many individual cells were located between the two compartments, segmentation was done separately. TPLSM images were processed by Imaris software (Bitplane).

Single cell *Igh* sequencing

Single PP was harvested from *Aicda*$^{Cre/+}$Rosa26$^{Stop\text{-}tdTomato}$ and processed for flow cytometry analysis. Cell suspensions were stained for dump (CD4, CD8, GR-1, F4/80) and gated as dump^{-}tdTomato^{+}B220^{+}GL-7^{+}FAS^{+}CCR6^{-}IgA^{+} or tdTomato^{+}B220^{+}GL-7^{-}FAS^{+}CCR6^{+}IgA^{+} representing GC or SED cells, respectively. Cell sorting was performed using a FACS Aria cell sorter (BD Bioscience). For total VDJ sequencing of Igα heavy chains, GC and SED derived B cells were sorted into 96 well plates containing lysis buffer (PBS containing 3 U/µl RNAsin, 10 mM dithiothreitol –DTT). cDNA was purified using random primers (NEB) as previously described [49]. Igα heavy chain sequence was amplified twice using primers for the Igα constant region (5′-ATCAGGCAGCCGATTATCAC-3′ for the first reaction and 5’-GAGGTGCAGCTGCAGGAGTCTGG-3′ for the second reaction)[42] together with a mix of primers for the variable region (Table S2)[50]. The PCR products were sequenced and analyzed for CDR3 using web-based IgBlast and IMGT tools. Sequence alignment was

performed using SnapGene software (GSL Biotech). For schematic representation of the results, sequences derived from single cells were clustered according to their CDR3 region and presented as percent of the total sequenced cells. Primer-derived mutations were excluded from the analysis.

Igh lineage analysis

Ig Fasta sequences were aligned against the IMGT mouse heavy chain gene database (Sep. 2017) using NCBI IgBlast (version 1.7.0)[51]. Post processing of IgBlast output, and clonal clustering were performed using Change-O v0.3.7 (http://changeo.readthedocs.io/)[52], Alakazam v0.2.8 (http://alakazam.readthedocs.io), SHazaM v0.1.8 (http://shazam.readthedocs.io), and custom scripts within the R statistical computing environment, as follows. V(D)J sequences were assigned to clonal groups by partitioning sequences based on sequence similarity of IGHV gene annotations, IGHJ gene annotations, and junction region lengths. Within these groups, sequences differing from one another by a hamming distance of 0.2 within the junction region were defined as clones by single-linkage clustering. Distances were measured and normalized by the length of the junction region. The clonal distance threshold was determined by manual inspection to identify the local minima between the two modes of the within-sample bimodal distance-to nearest histogram. Full-length germline sequences were reconstructed for each clonal cluster with D segment and N/P regions masked (replaced with Ns), with any ambiguous gene assignments within clonal groups resolved by the majority rule. Lineage trees were constructed for each clone having at least two unique sequences using PHYLIP (v3.695)[53] and Alakazam.

Statistics and Reproducibility

Statistical significance was determined with Graphpad Prism Version 5.0 using the tests indicated in each figure. All null hypothesis testing was performed with a 95% confidence interval; df, degrees of freedom. In Fig. 1 two-tailed Student's t test was performed with t = 5.3, df = 26 in Fig. 1b, t = 5.6, df = 63 (SED) and t = 4.0, df = 63 (GC) in Fig. 1c. For Fig. 2 differences in SED and GC volumes were calculated using one-way ANOVA with Bonferroni posttest, df = 3, F = 8.5 in (c). For Fig 2d, two-tailed Student t test, t = 1.9, df = 20 (SED) and t = 6.7, df = 20 (GC). For Fig. 2e t = 7.4, df = 10 (no competition) and t = 5.7, df = 8 (competition), two-tailed Student's t test. For Fig. 2f, df = 2, F=294.3. For Fig. 2g, t = 0.8, df = 10, two-tailed Student's t test. For Fig. 2h. t = 0.9, df = 10, two-tailed Student's t test. For Fig. 3b,c, df = 2, F = 16.3 (SED) and df = 2, F = 54.0, one-way ANOVA with Bonferroni posttest. For Fig. 4, t = 1.7, df = 68 in a (SED, no competition), t = 0.3, df = 67 (GC, no competition), t = 1.6, df = 110 (SED, competition), t = 11.54, df = 110 (GC, competition), two-tailed Student's t test. For Fig. 5, t = 2.3, df = 10 in (c), two-tailed Student's t test; df = 3, F = 10.9 in (d) and df = 3, F = 42.3 in (f), one-way ANOVA with Bonferroni posttest. For Fig.6, t = 24.5, df = 10 in (a), t = 11.6, df = 10 in (b), two-tailed Student's t test; df = 2, F = 24.6 in (c), df = 2, F = 14.4 in (d), one-way ANOVA with Bonferroni posttest; t = 0.5, df = 10 in (e) and (f), two-tailed Student's t test. In Fig. 7d, t = 9.0, df = 342, two-tailed Student's t test.

Data availability: All BCR sequencing data generated in this manuscript have been deposited in the European nucleotide archive (ENA) under accession number PRJEB30525. Custom scripts used for data analysis are available upon request. All other data are available in the main text or the supplementary materials.

Ethical compliance: The experiments performed in this study were approved by the Weizmann Institute Animal Care and Use Committee (IACUC) and followed all relevant ethical regulations.

Methods References

44. Rakoff-Nahoum, S., Paglino, J., Eslami-Varzaneh, F., Edberg, S. & Medzhitov, R. Recognition of Commensal Microflora by Toll-Like Receptors Is Required for Intestinal Homeostasis. *Cell* **118,** 229–241 (2004).

45. Dahan, R. *et al.* Therapeutic Activity of Agonistic, Human Anti-CD40 Monoclonal Antibodies Requires Selective FcγR Engagement. *Cancer Cell* **29,** 820–831 (2016).

46. Gupta, J. & Nebreda, A. R. Analysis of Intestinal Permeability in Mice. *Bio-protocol* **4,** e1289 (2014).

47. Li, W., Germain, R. N. & Gerner, M. Y. Multiplex, quantitative cellular analysis in large tissue volumes with clearing-enhanced 3D microscopy (C $_e$ 3D). *Proc. Natl. Acad. Sci.* **114**, E7321–E7330 (2017).

48. Shulman, Z. *et al.* T follicular helper cell dynamics in germinal centers. **341,** 673–677 (2013).

49. Von Boehmer, L. *et al.* Sequencing and cloning of antigen-specific antibodies from mouse memory B cells. *Nat. Protoc.* **11,** 1908–1923 (2016).

50. Ho, I. Y. *et al.* Refined protocol for generating monoclonal antibodies from single human and murine B cells. *J. Immunol. Methods* **438,** 67–70 (2016).

51. Ye, J., Ma, N., Madden, T. L. & Ostell, J. M. IgBLAST: an immunoglobulin variable domain sequence analysis tool. *Nucleic Acids Res.* **41,** 34–40 (2013).

52. Gupta, N. T. *et al.* Change-O: A toolkit for analyzing large-scale B cell immunoglobulin repertoire sequencing data. *Bioinformatics* **31,** 3356–3358 (2015).

53. Felsenstein, J. Using the quantitative genetic threshold model for inferences between and within species. *Philos. Trans. R. Soc. B Biol. Sci.* **360**, 1427–1434 (2005).

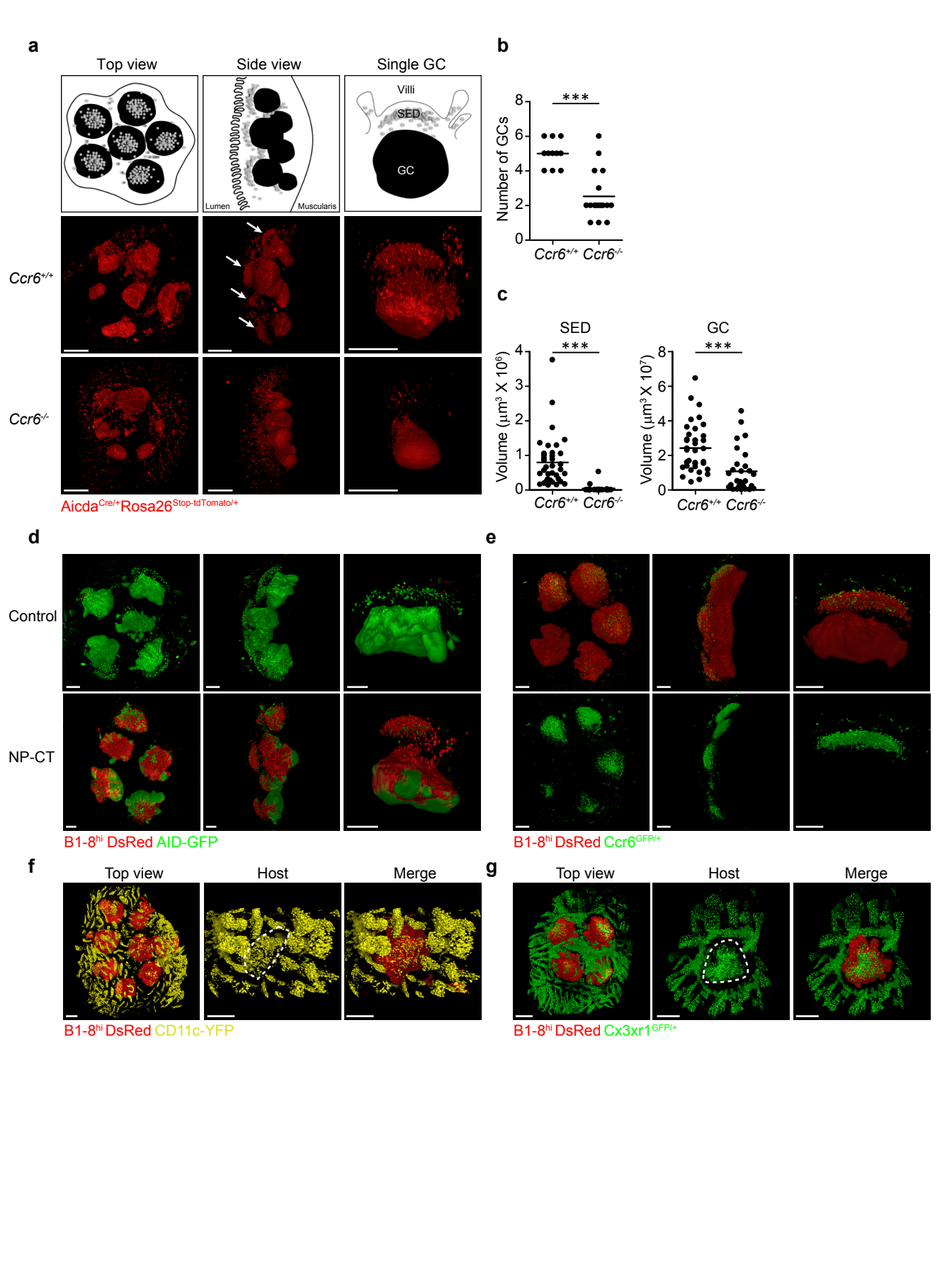
a
Top view
Side view
Single GC
Villi
SED
GC
Lumen
Muscularis
Ccr6+/+
Ccr6-/-
AicdaCre/+Rosa26Stop-tdTomato/+
b
Number of GCs
***
Ccr6+/+
Ccr6-/-
c
SED
GC
***
Volume (μm3 X 10^6)
Volume (μm3 X 10^7)
d
Control
NP-CT
B1-8hi DsRed AID-GFP
e
B1-8hi DsRed Ccr6GFP/+
f
Top view
Host
Merge
B1-8hi DsRed CD11c-YFP
g
Top view
Host
Merge
B1-8hi DsRed Cx3xr1GFP/+

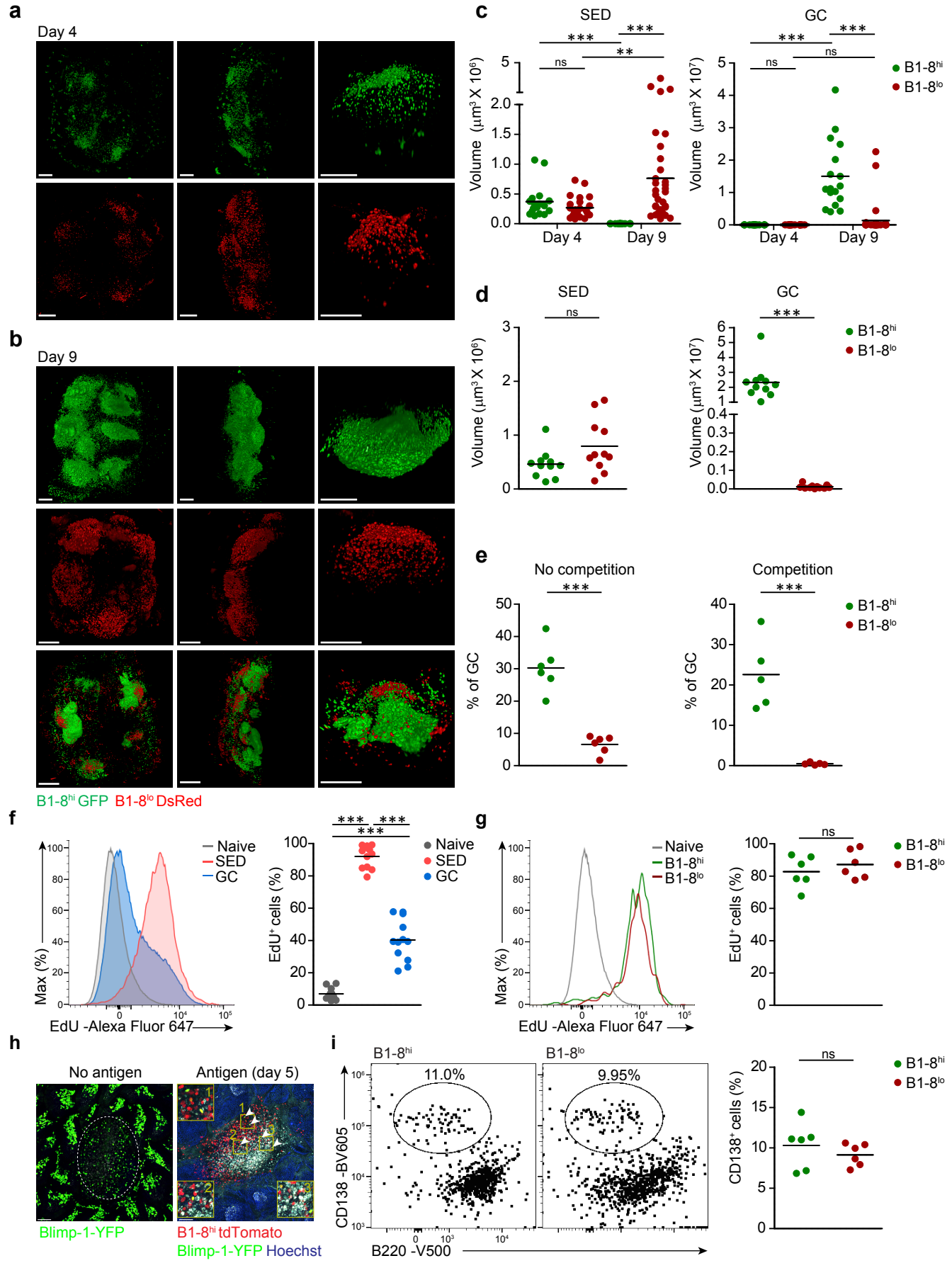
a
Day 4
b
Day 9
B1-8hi GFP B1-8lo DsRed
c
SED
GC
Volume (µm3 X 106)
Volume (µm3 X 107)
Day 4
Day 9
B1-8hi
B1-8lo
d
SED
GC
e
No competition
Competition
% of GC
f
Naive
SED
GC
Max (%)
EdU -Alexa Fluor 647
EdU+ cells (%)
g
B1-8hi
B1-8lo
h
No antigen
Antigen (day 5)
Blimp-1-YFP
B1-8hi tdTomato
Blimp-1-YFP Hoechst
i
11.0%
9.95%
CD138 -BV605
B220 -V500
CD138+ cells (%)

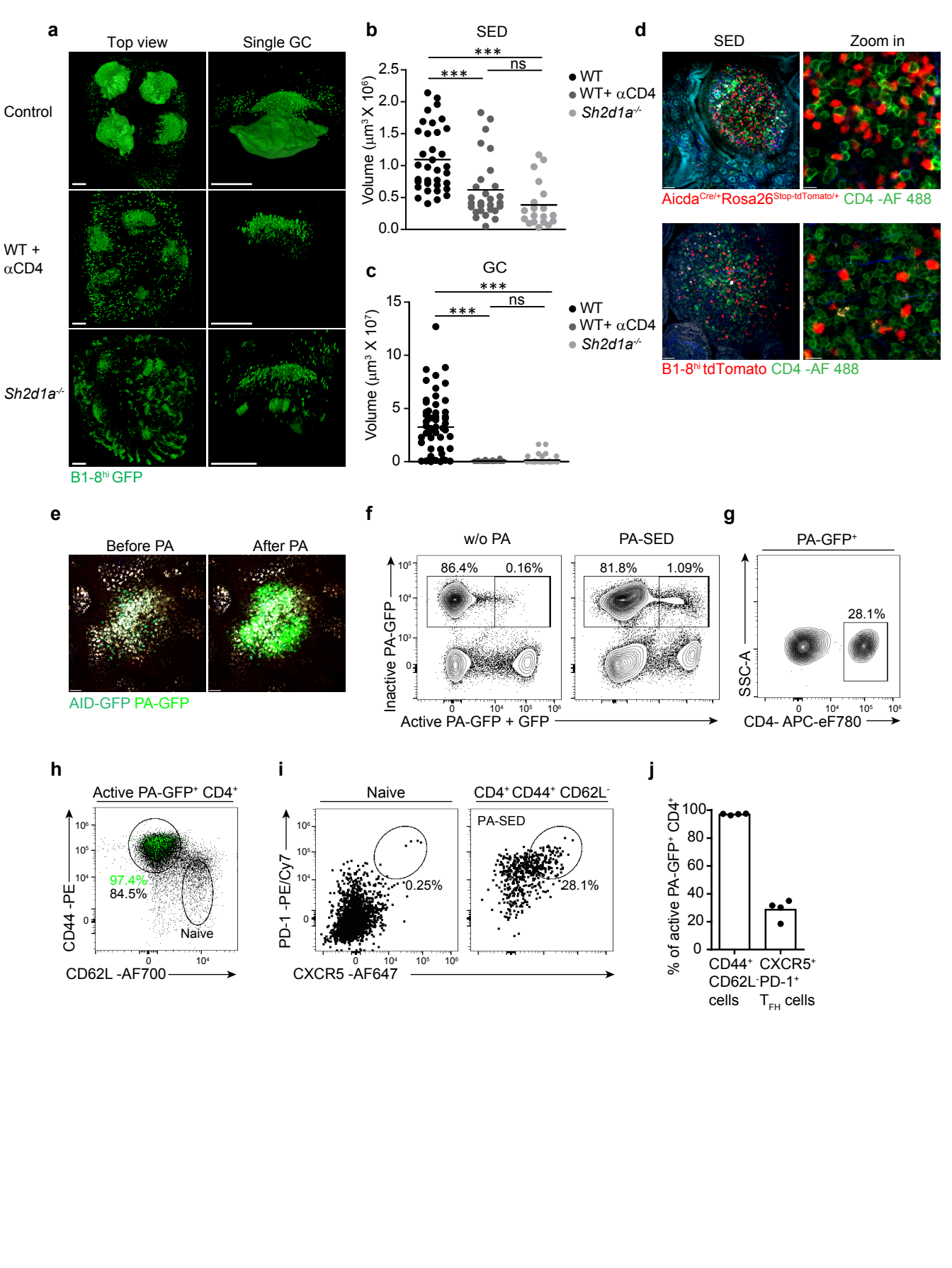
a
Top view
Single GC
Control
WT +
αCD4
Sh2d1a-/-
B1-8hi GFP
b
SED
***
***
ns
Volume (μm3 X 10^6)
2.5
2.0
1.5
1.0
0.5
0.0
WT
WT+ αCD4
Sh2d1a-/-
c
GC
***
***
ns
Volume (μm3 X 10^7)
15
10
5
0
WT
WT+ αCD4
Sh2d1a-/-
d
SED
Zoom in
AicdaCre/+Rosa26Stop-tdTomato/+ CD4 -AF 488
B1-8hi tdTomato CD4 -AF 488
e
Before PA
After PA
AID-GFP PA-GFP
f
w/o PA
PA-SED
86.4%
0.16%
81.8%
1.09%
Inactive PA-GFP
Active PA-GFP + GFP
g
PA-GFP+
28.1%
SSC-A
CD4- APC-eF780
h
Active PA-GFP+ CD4+
97.4%
84.5%
Naive
CD44 -PE
CD62L -AF700
i
Naive
CD4+ CD44+ CD62L-
PA-SED
0.25%
28.1%
PD-1 -PE/Cy7
CXCR5 -AF647
j
% of active PA-GFP+ CD4+
100
80
60
40
20
0
CD44+ CD62L- cells
CXCR5+ PD-1+ TFH cells

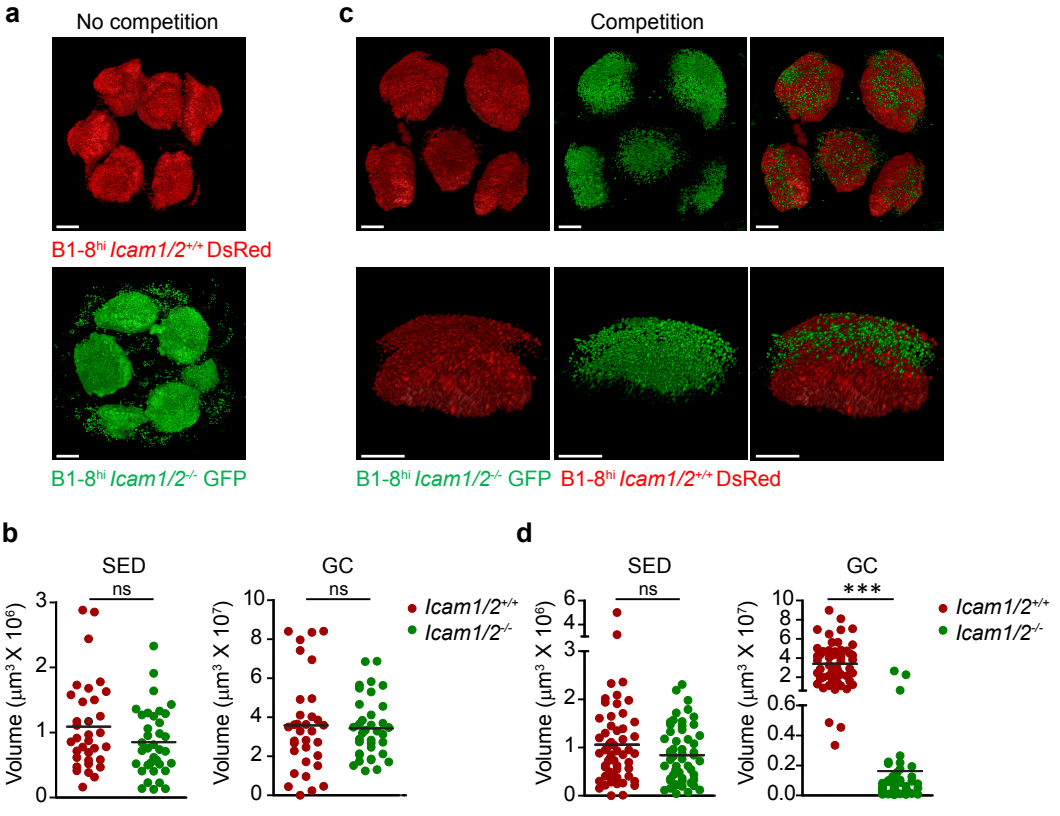
a
No competition
B1-8hi Icam1/2+/+ DsRed
B1-8hi Icam1/2-/- GFP
c
Competition
B1-8hi Icam1/2-/- GFP
B1-8hi Icam1/2+/+ DsRed
b
SED
GC
ns
ns
Volume (µm3 X 10^6)
Volume (µm3 X 10^7)
Icam1/2+/+
Icam1/2-/-
d
SED
GC
ns
***
Volume (µm3 X 10^6)
Volume (µm3 X 10^7)
Icam1/2+/+
Icam1/2-/-

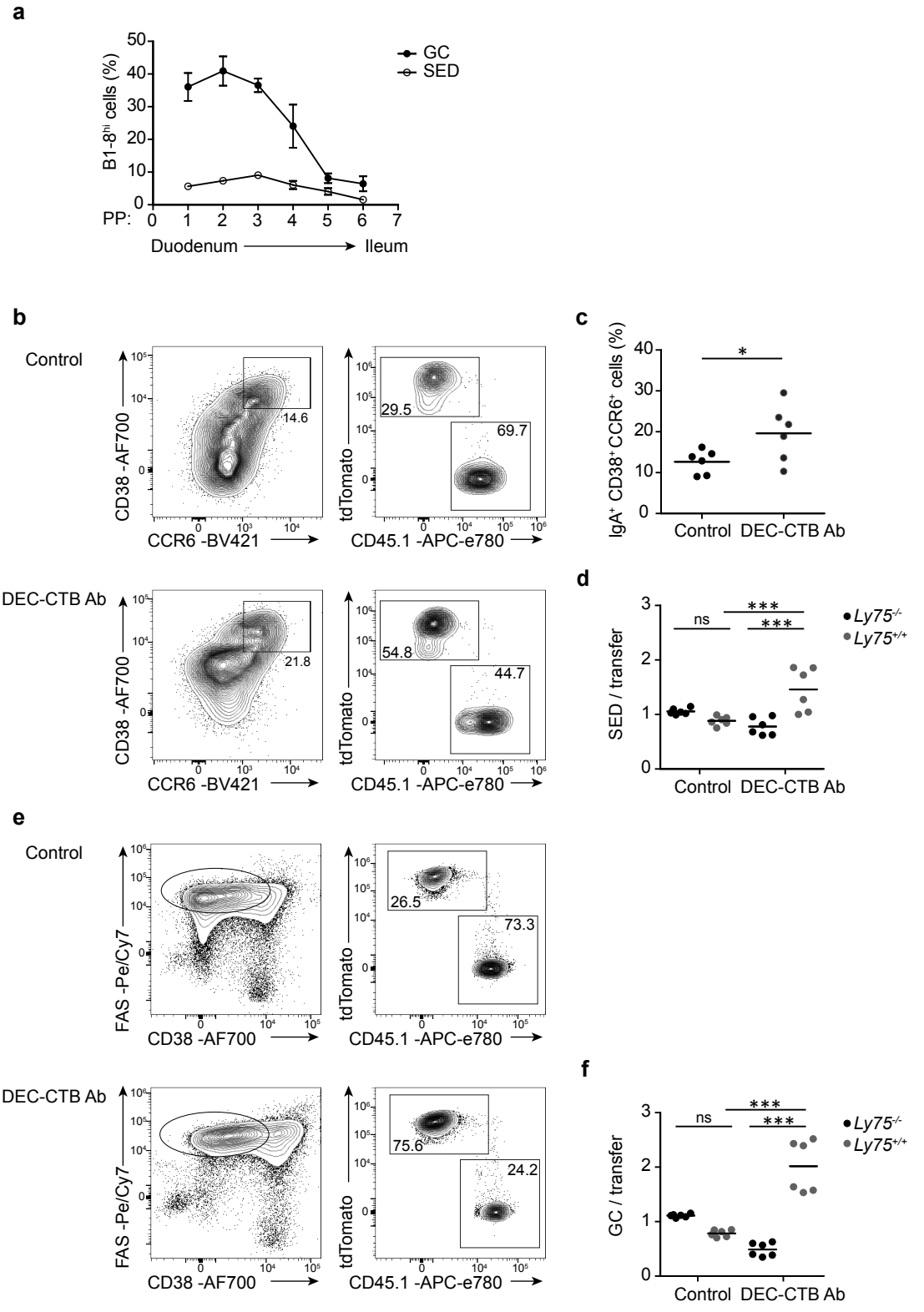
a
B1-8hi cells (%)
GC
SED
PP:
Duodenum
Ileum
b
Control
DEC-CTB Ab
CD38 -AF700
CCR6 -BV421
tdTomato
CD45.1 -APC-e780
14.6
29.5
69.7
21.8
54.8
44.7
c
IgA+ CD38+ CCR6+ cells (%)
Control
DEC-CTB Ab
d
SED / transfer
ns
Ly75-/-
Ly75+/+
e
FAS -Pe/Cy7
26.5
73.3
75.6
24.2
f
GC / transfer

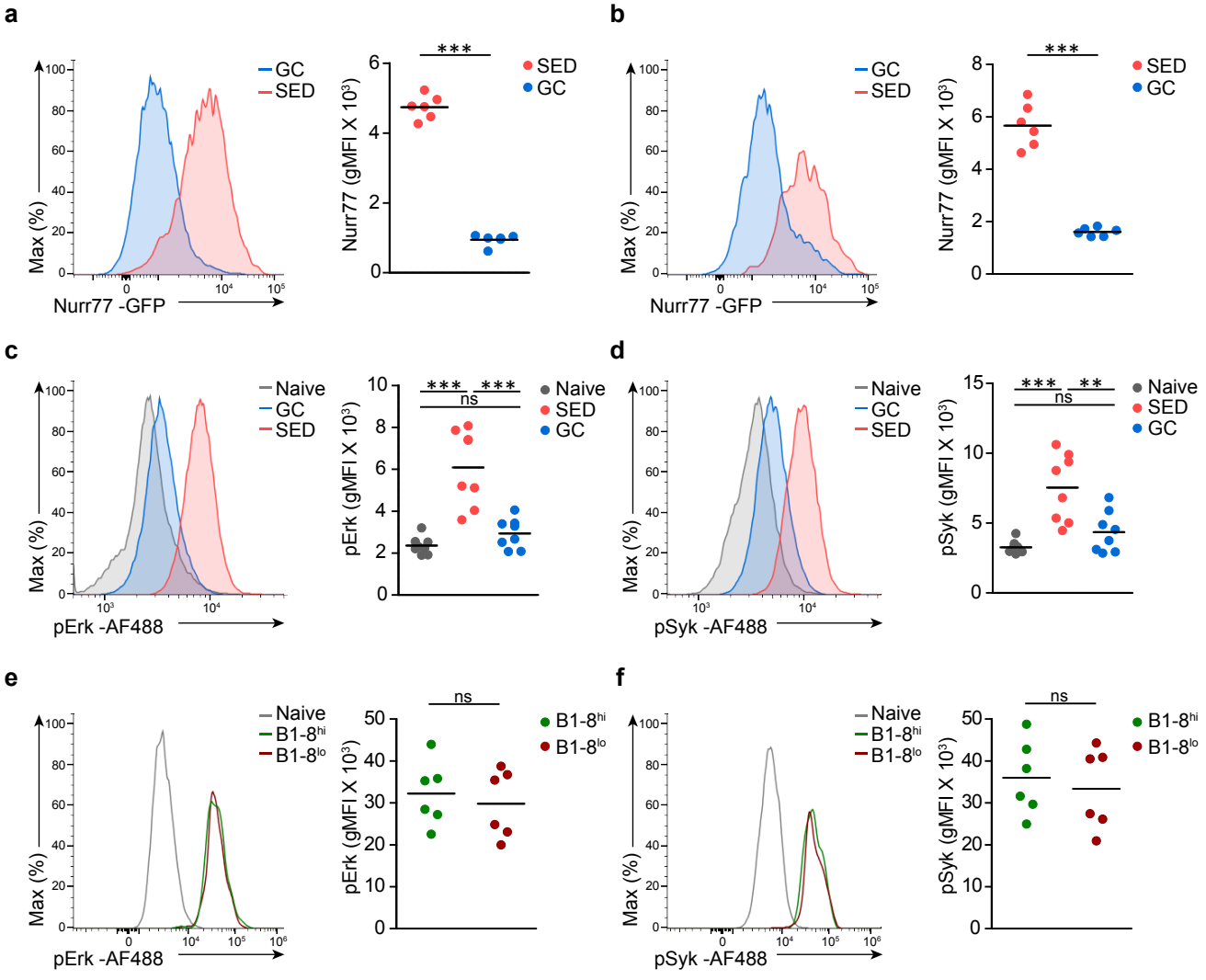
a
GC
SED
Max (%)
Nurr77 -GFP
***
SED
GC
Nurr77 (gMFI X 10³)
b
GC
SED
Max (%)
Nurr77 -GFP
***
SED
GC
Nurr77 (gMFI X 10³)
c
Naive
GC
SED
Max (%)
pErk -AF488
*** ***
ns
Naive
SED
GC
pErk (gMFI X 10³)
d
Naive
GC
SED
Max (%)
pSyk -AF488
*** **
ns
Naive
SED
GC
pSyk (gMFI X 10³)
e
Naive
B1-8hi
B1-8lo
Max (%)
pErk -AF488
ns
B1-8hi
B1-8lo
pErk (gMFI X 10³)
f
Naive
B1-8hi
B1-8lo
Max (%)
pSyk -AF488
ns
B1-8hi
B1-8lo
pSyk (gMFI X 10³)

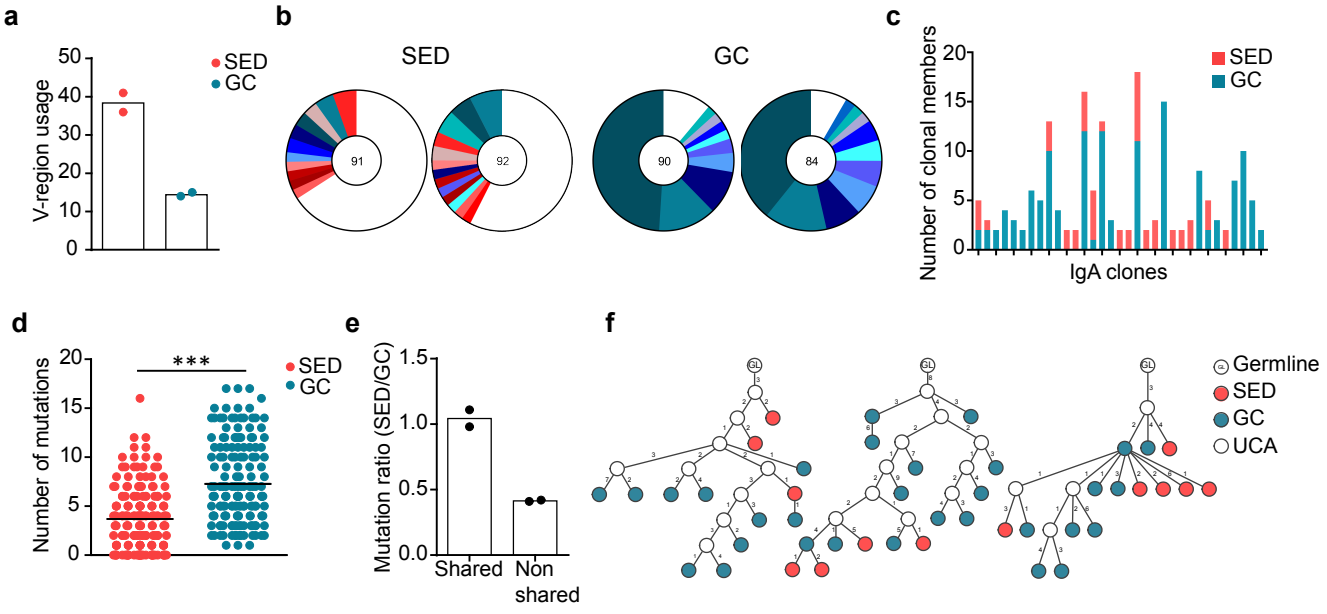
a
V-region usage
SED
GC
b
SED
GC
91
92
90
84
c
Number of clonal members
IgA clones
SED
GC
d
Number of mutations
***
SED
GC
e
Mutation ratio (SED/GC)
Shared
Non shared
f
Germline
SED
GC
UCA